JOURNAL OF AIRCRAFT
Vol. 41, No. 6, November–December 2004

Simulation of Flow About Rotating Forebodies at High Angles of Attack

S. Saephan* and C. P. van Dam†
University of California, Davis, California 95616-5294
C. M. Fremaux‡
NASA Langley Research Center, Hampton, Virginia 23681
and
T. DalBello§
University of Toledo, NASA Glenn Research Center, Cleveland, Ohio 44135

A Reynolds-averaged Navier–Stokes flow solver is used to predict the forces and moments on forebody models at high angle-of-attack rotary conditions. Cases simulated using either a circular or square ogive at an angle of attack of 60 deg, freestream Mach number of 0.21, and Reynolds number based on body diameter of approximately two million are presented and compared against wind-tunnel data from rotary testing on generic forebody models conducted by NASA Langley Research Center and the Defence Research Agency in the United Kingdom. The simulations provide insight into the flow characteristics at steady rotary conditions.

Nomenclature

b	=	reference body length (36 in.)
C_A	=	axial-force coefficient in body axis, axial-force/$(\frac{1}{2}\gamma p_\infty M_\infty^2 S)$
C_l	=	rolling-moment coefficient in body axis, rolling-moment/$(\frac{1}{2}\gamma p_\infty M_\infty^2 Sb)$
C_m	=	pitching-moment coefficient in body axis, pitching-moment/$(\frac{1}{2}\gamma p_\infty M_\infty^2 SD)$
C_N	=	normal-force coefficient in body axis, normal-force/$(\frac{1}{2}\gamma p_\infty M_\infty^2 S)$
C_n	=	yawing-moment coefficient in body axis, yawing-moment/$(\frac{1}{2}\gamma p_\infty M_\infty^2 Sb)$
C_p	=	pressure coefficient in body axis, $(p - p_\infty)/(\frac{1}{2}\gamma p_\infty M_\infty^2)$
C_Y	=	side-force coefficient in body axis, side-force/$(\frac{1}{2}\gamma p_\infty M_\infty^2 S)$
D	=	reference body diameter (6 in.)
M_∞	=	freestream Mach number (0.21)
p_∞	=	freestream static pressure
R	=	radius of curvature
Re_D	=	Reynolds number based on body diameter
S	=	reference area, $S = b \times D$ (216 in.^{2})
V_∞	=	freestream velocity
α	=	angle of attack (60 deg)
γ	=	ratio of specific heats
θ	=	circumferential angle
Ω	=	angular velocity about spin axis
$\Omega b/2V_\infty$	=	spin coefficient, positive for clockwise spin

Received 16 August 2002; revision received 11 March 2004; accepted for publication 17 February 2004.

*Graduate Student, Department of Mechanical and Aeronautical Engineering, One Shields Avenue; ssaephan@ucdavis.edu.

†Professor, Department of Mechanical and Aeronautical Engineering, One Shields Avenue; cpvandam@ucdavis.edu.

‡Research Engineer, Mail Stop 153, Vehicle Dynamics Branch; Charles.M.Fremaux@nasa.gov.

§Senior Research Associate, 21000 Brookpark Road; teryn@grc.nasa.gov.

Introduction

ACCURATE determination of the stability and control characteristics of an aircraft is critical to the safety of that aircraft. The flight envelope of some high-performance aircraft often pushes the limits on angle of attack and rapid motion maneuvers. At these flight conditions the flow about the aircraft tends to be unsteady and separated, and the variations in the forces and moments with angle of attack or motion rate are often nonlinear. During the development process of these aircraft, numerous hours are spent testing scaled models in wind tunnels to determine the stability and control characteristics. Much of this testing is conducted using models of simplified geometry at Reynolds numbers much lower than typical flight Reynolds number. However, the sensitivity of the forces and moments to Reynolds number makes these empirical approaches to predict dynamic characteristics at full-scale high-angle-of-attack conditions a challenging task. Both Haines[1] and Polhamus[2] published reviews of Reynolds-number effects on flow over bodies.

Much of the wind-tunnel testing is conducted with special equipment designed for this purpose and includes both oscillatory and rotary test techniques. A critical examination of the rotary balance technique for the analysis of high-angle-of-attack dynamic behavior of aircraft was presented by the North Atlantic Treaty Organization's Advisory Group for Aerospace Research and Development.[3] This wind-tunnel test technique involves a coning motion (a continuous rolling motion of the model about the freestream velocity vector) as depicted in Fig. 1. It was developed to provide information on the effects of angular rates on the aerodynamic forces and moments acting on the aircraft in flight. The rotary balance apparatus as shown in Fig. 1 is complex because it must be capable of measuring forces and moments for the range of rotation rates experienced by high-performance aircraft. Major problems encountered in the application of this test technique include test equipment interference, wind-tunnel wall effects, equipment blockage ratio, and Reynolds-number scaling effects in addition to the difficulty of conducting detailed flow measurements such as surface pressures.

This study is motivated by the need of industry to quickly and inexpensively determine stability and control characteristics of new aircraft configurations without solely having to resort to wind-tunnel experiments. In particular, rotary balance testing at high Reynolds numbers is complex because of the high structural loads imposed on the model and the rotary test apparatus. The high loading is the result of the combined effects of high dynamic pressure of the wind-tunnel flow and the high angular velocities required to match the flow velocities for a given spin coefficient. The potentially cheaper

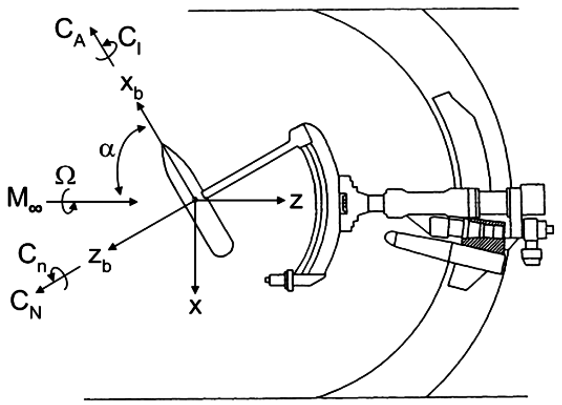

Fig. 1 Rotary apparatus setup and ogive model coordinate axes: y_b and y axes point into the page to form right-handed coordinate systems.

and faster aspects of computational fluid dynamics (CFD) make it a valuable tool to supplement wind-tunnel experiments, if it can be proven to be reliable under dynamic conditions. To that end, a Reynolds-averaged Navier–Stokes (RANS) flow solver is applied to predict the flow characteristics about circular and square cross-section forebody models at high-angle-of-attack rotary conditions.

In the mid-1990s, rotary balance experiments were conducted on isolated circular and square cross-section ogive models at angles of attack of 60 and 90 deg over a range of Reynolds numbers from 0.08×10^6 to 2.25×10^6 based on the maximum body diameter.[4,5] The purpose of these experiments was to determine the effects of Reynolds number, spin coefficient, and forebody geometry on the aerodynamic characteristics of the models. These tests were unique in so far that this was the first time that surface-pressure distributions were measured under rotary conditions in a pressurized wind-tunnel. A second objective of these experiments was to provide a database for the development and validation of high-angle-of-attack computational methods. This database forms the basis for the computational investigations of this paper.

Numerical simulations of dynamic applications are only in their infancy. Inviscid methods and viscous/inviscid interaction methods tend to be inapplicable because of the strong viscous effects and the large regions of separated flow that occur at high-angle-of-attack conditions. Also, methods based on the Euler equations only predict vortex formation originating from flow separation at sharp edges and ignore the vortices that originate from flow separation on smooth surfaces such as the ogive forebodies considered in this study. Currently, the only affordable approach for the prediction of aircraft dynamics at high angles of attack is based on the three-dimensional Reynolds-averaged Navier–Stokes equations. Large eddy simulations (LES) and hybrid RANS/LES methods are still under development and being advertised as possibly a more accurate tool, but the computational costs are prohibitively expensive and unaffordable by most for any type of design work.[6] Most of the developments in CFD have concentrated on static problems, such as computation of lift and drag of aircraft at stationary conditions. Relatively few researchers have explored the application of CFD methods to dynamic aircraft problems.

Several recent studies provide novel approaches to deal with body motion in CFD simulations. Chaderjian and Schiff[7] analyzed the wing-rock problem of delta wings at high angle of attack using a single grid technique. Sturek et al.,[8] Weinacht and Sturek,[9] Weinacht et al.,[10] and Weinacht[11] have analyzed the damping characteristics of various motions (including coning motion) of projectiles at supersonic conditions. Ludlow and Qin[12] have computed the pitch damping characteristics of blunt projectiles at high Mach numbers. Ahmad and Duque[13] analyzed the flow around a rotating helicopter rotor using OVERFLOW-Rotorcraft. Nygaard and Meakin[14] simulated a spinning missile with dithering canards with OVERFLOW-D.

In the present study, both OVERFLOW-Rotorcraft and OVERFLOW-D are used to numerically simulate several of the test

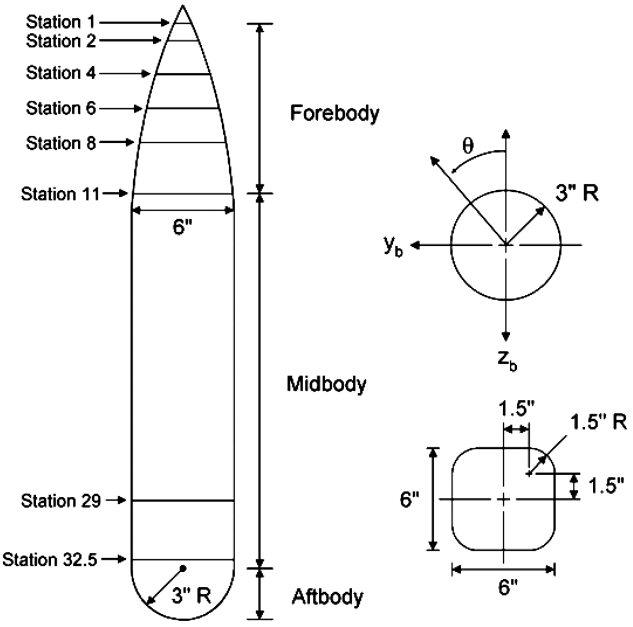

Fig. 2 Diagram of ogive models with planform and cross-sectional dimensions and axial location of pressure ports.

cases investigated by Pauley et al.[5] In the next few sections, the forebody models as well as the experimental setup used to generate the database are discussed, followed by details of the computational grids, flow solver, numerical results, and discussion.

Model Geometry and Test Setup

In the early to mid-1990s, wind-tunnel experiments were conducted by the British Defence Research Agency (DRA) and NASA Langley, which measured forces and moments as well as surface pressure for forebody models at various angles of attack and rotary conditions. The tests were conducted in the DRA's 13×9 ft atmospheric wind tunnel at Bedford and 8×6 ft pressurized wind tunnel at Farnborough. These tunnels provided a freestream Mach number range from 0.024 to 0.21 and a unit Reynolds number range from 0.15 to 4.5×10^6 per foot for these tests.

Several model geometries were wind-tunnel tested, but only two are simulated for comparison. Both geometries have an ogive forebody, tubular midbody, and hemispherical aftbody. The difference between the two models is their cross-sectional shape. One model has a circular cross section, whereas the other model has a square with rounded corners cross section. Figure 2 shows the models including their dimensions.

The test models had six circumferential rows of surface-pressure taps on the forebody and two rows near the aftbody with the rows designated as stations 1, 2, 4, 6, 8, 11, 29, and 32.5. The station locations are shown in Fig. 2.

The models were attached to the wind-tunnel's rotary balance apparatus via a sting at its lengthwise midpoint. More detailed information about the test models and experimental setup can be found in Pauley et al.[5]

Flow Solver

OVERFLOW is a Reynolds-averaged Navier–Stokes flow solver developed by Buning et al.[15] for structured grids. The flow solver itself is very robust and comprehensive in the sense that it provides a wide selection of numerical schemes, boundary conditions, and turbulence models in addition to its ability to solve a wide range of flow conditions and geometry configurations. For this study, central differencing is used for the spatial terms. To advance the solution in time, the lower-upper symmetric Gauss–Seidel (LU-SGS)[16] scheme is used because it is very robust. An alternative to LU-SGS is the Beam–Warming[17] method, hereafter referred to as the ARC3D scheme to be consistent with the name used in the OVERFLOW

manual. The turbulence models that have been incorporated into the solver include the algebraic Baldwin–Lomax[18] model and the one-equation Spalart–Allmaras[19] model.

Like other software, numerous versions of the flow solver have been created and are in use. Two versions of OVERFLOW were used to obtain the results presented in this paper.

The Army/NASA Rotorcraft Division enhanced the basic OVERFLOW solver by adding rotorcraft-specific capabilities,[20] which include a source-term formulation to calculate steady rotary flow problems.[21] The source-term formulation allows for the simulation of a body under constant rotation using a static grid in a noninertial reference frame. This feature is effective in calculating steady-state solutions for the present study's dynamic forebody problems and resulted in significant savings of computational time. The source-term formulation has been investigated by others including Park and Green[22] and Zhong and Qin.[23]

The source-term capability in OVERFLOW-Rotorcraft is limited to rotation about the z-axis only and therefore restricts the orientation of the computational coordinate system. However, the experiments measured forces and moments with respect to the body-fixed coordinate system shown in Fig. 1. The orientations of the computational and experimental coordinate systems are shown in Fig. 1. The computational axis labels have no subscript while the experimental axis labels have a subscript b. All computational results are transformed to the body-fixed reference frame.

Recently, OVERFLOW and the derivative rotorcraft version have been superceded by OVERFLOW-D, which has been significantly and specifically enhanced to accommodate dynamic applications with multiple bodies and six-degrees-of-freedom motion. Other improvements to the code include automatic off-body grid generation, force and moment computations, hole cutting, and domain connectivity between overset grids.[14] OVERFLOW-D can be compiled with Message Passing Interface* for parallel computing.

Computational Grid Topology

The computational grids for the ogive models are generated using the Chimera Grid Tools[24] grid-generation package. OVERGRID[25] is the graphical user interface for the various grid-generation modules included in the Chimera Grid Tools package.

The surface geometries are generated based on physical measurements of the ogive test models by the Quality Assurance and Inspection Branch at NASA Langley Research Center. Numerous circumferential sets of coordinates were measured on the forebody to obtain an accurate surface representation. Coordinates describing the midbody and aftbody cross sections are computed based on analytical descriptions provided by Pauley et al.[5] The measured forebody and computed midbody and aftbody coordinates supplied the information needed by various Chimera modules to generate the computational surface grids for both the circular and square ogive models.

The surface grid is defined by 181 equally spaced points in the circumferential direction and 130 stretched points in the axial direction. Points 1 and 181 on the circumferential axis coincide to complete the periodic closed surface. In the axial direction, the grid points are concentrated near the very tip of the forebody and rear hemispherical cap. The volume grids are generated with HYPGEN,[26] a hyperbolic volume grid generator within the Chimera package. The first four points off the surface have a constant spacing of 3.33×10^{-4} diameters. Starting at normal grid point number five, the normal grid spacing is stretched with a stretching ratio of approximately 1.25 until the outer boundary is reached at 50 diameters, for a total of 54 points in the normal direction. Hence, the total number of grid points is approximately 1.25 million.

Analysis Methodology

Although the experimental surface-pressure data are used as the basis for all forebody flow comparisons, it was revealed that the wind-tunnel experiments had an inaccurate reference pressure,[27] which resulted in surface-pressure coefficients that were too high including values greater than unity in the flow attachment region, something that is physically impossible at low-Mach-number test conditions. The reference pressure problem was not uncovered until after the actual experiments were completed. The magnitude of the error in the experimental data is not known, but the error is present in all of the data, and hence the overall relative pressure distributions are believed to be correct. Despite the reference pressure error, the data sets still provide reasonable comparisons with computational results. A more thorough discussion of this reference pressure problem is presented in Ref. 28.

For a more detailed comparison between the experimental and computational results, the computed surface pressures over the forebody region are integrated to determine the force and moment contributions of the forebody section. Similar integration of the experimental surface pressures over the exact region allow for a direct comparison of the forebody forces and moments. All reported forces and moments are in reference to the body-fixed axis system as shown in Fig. 1. The forebody forces and moments are different than those measured by the wind-tunnel balance. The balance measures the total forces and moments acting on the entire model, whereas the forebody forces and moments are just contributions from the forebody section. There is no way for the wind-tunnel balance to isolate the forebody contributions, and so the surface-pressure integration is necessary.

Convergence Criteria

Several criteria are used to determine the convergence of numerical simulations. The solution residual in terms of the L^2 norm is a measure of the numerical error for the discretized system of equations and would ideally diminish to machine zero. As the residual is decreasing, the forces and moments should be approaching steady-state values. Tandem tracking of the L^2 norm, forces, and moments reveals the development of the CFD solution. When the forces and moments change by less than 5% after an additional 500 iterations and the residual is reduced by several orders of magnitude, the simulation is considered converged. In all instances, the flow over the forebody region converges much more rapidly than that of the complete configuration. In fact, the forebody region is typically converged after only 30% of the total number of iterations.

Computational Results

The DRA wind-tunnel experiments included numerous test cases with different angles of attack, Reynolds numbers, spin coefficients, freestream Mach numbers, and model configurations. Select cases are solved numerically with OVERFLOW and compared to experimental results as the main objective of this study. The circular and square ogives are simulated as fully turbulent at the highest Reynolds number experimentally tested under several rotation rates. All cases are at an angle of attack of 60 deg, and $M_\infty = 0.21$. Results are discussed next.

The circular ogive configuration is simulated at three different spin coefficients of $\Omega b/(2V_\infty) = -0.2$, -0.1, or 0.0 and $Re_D = 2.08 \times 10^6$ with the Baldwin–Lomax[18] turbulence model. Figure 3 shows the convergence characteristics of the three simulations in terms of L^2 norm, side-force coefficient, and yawing-moment coefficient for the entire body. After 9000 iterations, the residuals are reduced by approximately three orders of magnitude, and the forces and moments, including the other components not shown, have converged. Table 1 shows the force and moment coefficients for the forebody section. Except for the side force and yawing moment, all of the other components have less than a 5% error relative to the experimental results. The errors in the side forces are generally smaller than errors in yawing moments as expected. Moments are more difficult to predict as they are more sensitive to variations in surface pressure far from the moment center. It should be emphasized that Fig. 3 and Table 1 depict different results. Figure 3 shows the side force and yawing moment acting on the whole model, whereas Table 1 lists the force and moment contributions from the forebody section only. The forebody section is labeled in Fig. 2.

*Software available online at http://www-unix.mcs.anl.gov/mpi/mpich/.

Table 1 Comparison of forebody (see Fig. 2 for forebody definition) force and moment coefficients for the circular ogive at $\alpha = 60$ deg, $M_\infty = 0.21$, and $Re_D = 2.08 \times 10^6$

	CFD			Experiment		
$\Omega b/2V_\infty$	−0.2	−0.1	0.0	−0.2	−0.1	0.0
C_N	−0.1404	−0.1400	−0.1404	−0.1419	−0.1411	−0.1414
C_A	−3.9468	−3.9478	−3.9480	−4.0730	−4.0717	−4.0710
C_Y	0.0269	0.0166	0.0089	0.0248	0.0193	0.0139
C_l	0.0002	0.0002	0.0002	0.0002	0.0002	0.0002
C_m	0.2619	0.2612	0.2618	0.2636	0.2624	0.2625
C_n	0.0065	0.0035	0.0011	0.0054	0.0037	0.0020

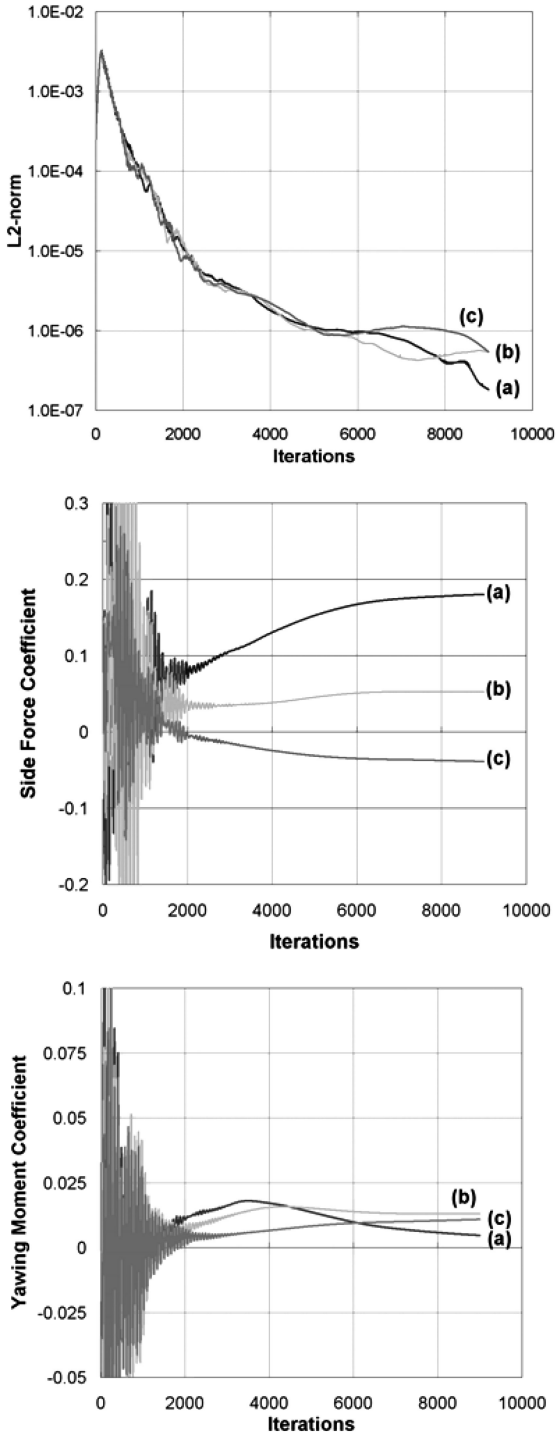

Fig. 3 Residual, side force, and yawing moment for the circular ogive at $\alpha = 60$ deg, $M_\infty = 0.21$, $Re_D = 2.08 \times 10^6$, and a) $\Omega b/(2V_\infty) = -0.20$, b) $\Omega b/(2V_\infty) = -0.10$, and c) $\Omega b/(2V_\infty) = 0.0$.

The axial-force coefficients are relatively large compared to all other force components, but that is because it is only the forebody contribution. The forebody section is not a closed surface in the axial direction, and all of the axial force contributions from the forebody act in the negative x_b direction. For the complete configuration including the midbody and aftbody sections (as defined in Fig. 2), the large negative axial force generated by the forebody will be mostly offset by a large positive axial force generated by the aftbody.

Figure 4 compares the surface-pressure distributions at stations 1, 4, 8, and 11. The general trend agreement between the measured and computed values is apparent. However, the computed pressures are slightly but noticeably shifted upwards when compared to the measured values. This small shift can be attributed primarily to the reference pressure error in the experimental data discussed earlier.

The square ogive configuration is also simulated with a spin coefficient of $\Omega b/(2V_\infty) = -0.2$, -0.1, or 0.0 and a slightly higher Reynolds number of $Re_D = 2.09 \times 10^6$. Forebody force and moment coefficients for all three square ogive cases are compared to experimental data in Table 2. The error in the side-force, pitching-moment, and yawing-moment coefficients is greater than 10%, but all other components are within a 10% range. Figure 5 compares the computed and measured forebody pressure distribution at four forebody stations for the $\Omega b/(2V_\infty) = -0.2$ case. Similar to the preceding case, the general trend agreement is present along with the shift in the experimental pressure coefficients, although the computations seem to overpredict the suction peaks and slightly shift their location.

Tables 1 and 2 depict nonzero side-force, rolling-moment, and yawing-moment coefficients for the cases with no rotation. There are several reasons why they should not be zero as confirmed by the nonzero values measured in the wind-tunnels. Neither of the two wind-tunnel models was perfectly symmetric, and whatever asymmetry was present in the wind-tunnel models was reproduced in the surface grids. This is the reason why the forebody section of the test models was extensively measured to obtain actual surface coordinates in lieu of using simple analytical descriptions. Even for nominally symmetric bodies the flow tends to become asymmetric in the angle-of-attack range from approximately 20 to 70 deg. At lower angles of attack, the flow remains symmetric, whereas at higher angles unsteady vortex shedding occurs. Hence, it is not unexpected that the side force, rolling moment, and yawing moment are nonzero at the stationary, $\alpha = 60$ deg condition for the bodies considered here.

Figure 6 compares the leeside vortex field at station 8 for both geometries at two spin coefficients. Rotation-rate effect is seen through the skewness of the vortices, with the $\Omega b/(2V_\infty) = -0.2$ cases showing more skewness than the $\Omega b/(2V_\infty) = -0.1$ cases as expected.

Discussion

The computational results presented show reasonable agreement with the experimental results in terms of forebody pressure distributions. Integration of the forebody surface pressures allows for the direct comparison of the forebody force and moment contributions. For the cases studied, the side force and yawing moment tended to have largest errors, which in some instances were as large as 40%.

Table 2 Comparison of forebody (see Fig. 2 for forebody definition) force and moment coefficients for the square ogive at $\alpha = 60$ deg, $M_\infty = 0.21$, and $Re_D = 2.09 \times 10^6$

	CFD			Experiment		
$\Omega b/2V_\infty$	−0.2	−0.1	0.0	−0.2	−0.1	0.0
C_N	−0.1904	−0.1913	−0.1917	−0.2166	−0.2142	−0.2134
C_A	−4.7448	−4.7460	−4.7462	−4.7797	−4.7701	−4.7569
C_Y	0.0786	0.0411	0.0040	0.0564	0.0302	0.0039
C_l	−0.0002	−0.0001	0.0000	−0.0001	0.0000	0.0000
C_m	0.3568	0.3578	0.3585	0.4078	0.4019	0.3998
C_n	0.0219	0.0113	0.0009	0.0156	0.0080	0.0007

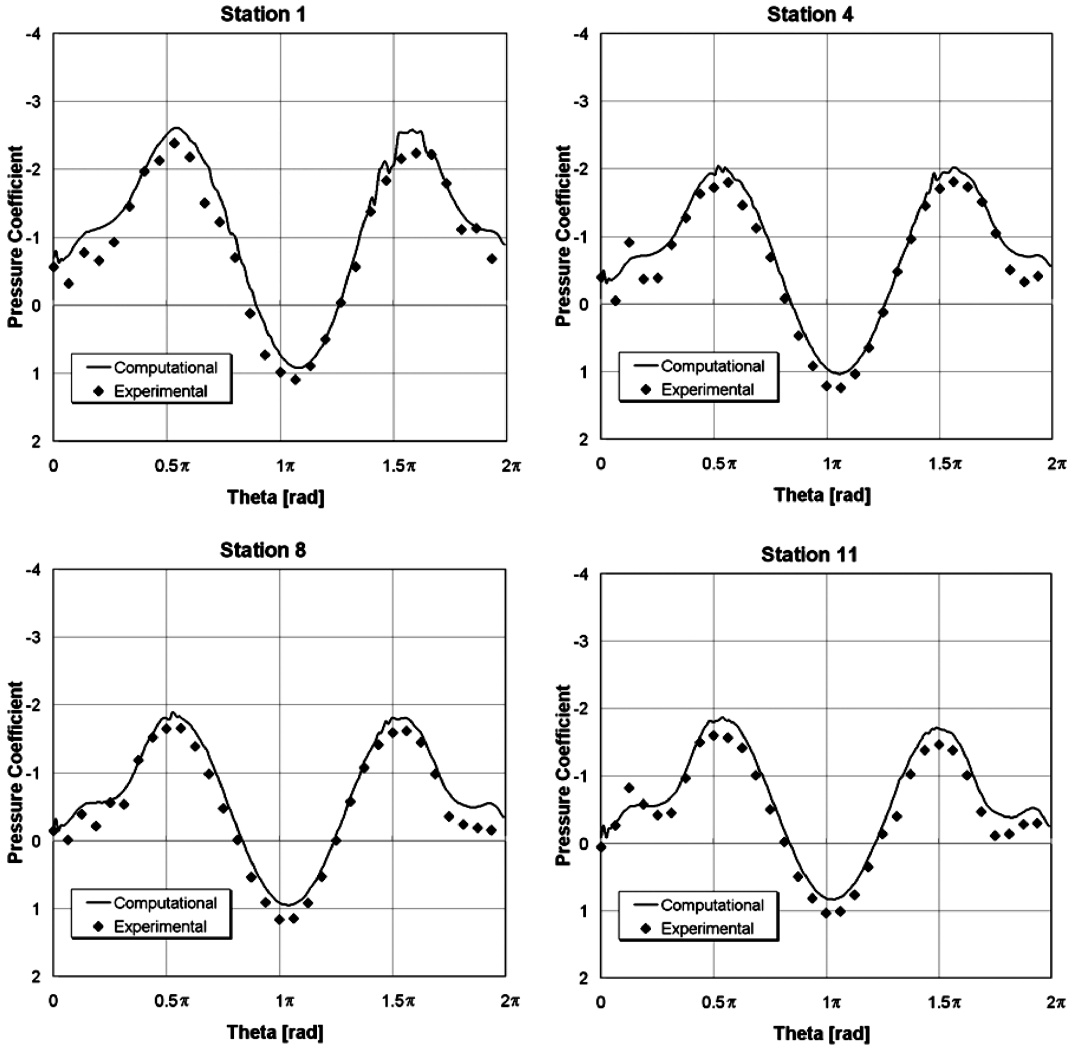

Fig. 4 Line plots of forebody pressure distribution for the circular ogive at $\alpha = 60$ deg, $M_\infty = 0.21$, $Re_D = 2.08 \times 10^6$, and $\Omega b/(2V_\infty) = -0.20$. $\theta = 0$ deg is the top or leeside of the model. (See Fig. 2 for station locations and theta orientation.)

The accuracy of CFD solutions depends on many factors, some of which include geometry representation, grid size, turbulence model, and transition prediction. Each of these issues will be addressed separately in the following.

The surface grids are believed to be fairly accurate in representing the geometry of the wind-tunnel models. As mentioned earlier, they are constructed based on detailed measurements of the forebody section of the actual wind-tunnel models and on analytical data for the mid and aft sections. For this study, neither the sting nor rotary balance apparatus is modeled. The sting and rotary rig can cause the vortices shed from the forebody to burst prematurely, thus affecting the forebody flow development. Flow in the immediate vicinity and downstream of the sting is certainly affected by the sting. Ericsson[29] showed that the sting on a wind-tunnel model has significant effects on the side force for high angles of attack. The presence of the sting alone can more than double the magnitude of side-force coefficient.

Grid size is always an issue for computational simulations. To ensure that the numerical solutions are not mesh dependent, several cases with smaller grid spacings are simulated and the forces and moments compared. The circumferential points that define the ogive surface collapsed into a single point at tip of the forebody and aftbody. As a result of the two collapsed points, singular axis poles emanate outwards from the two points in the volume grid. Refining the grid with this particular grid topology caused numerical instabilities in steady simulations with the rotational source term. To keep the single grid topology but avoid the numerical instability problem, it was necessary to switch to OVERFLOW-D to conduct

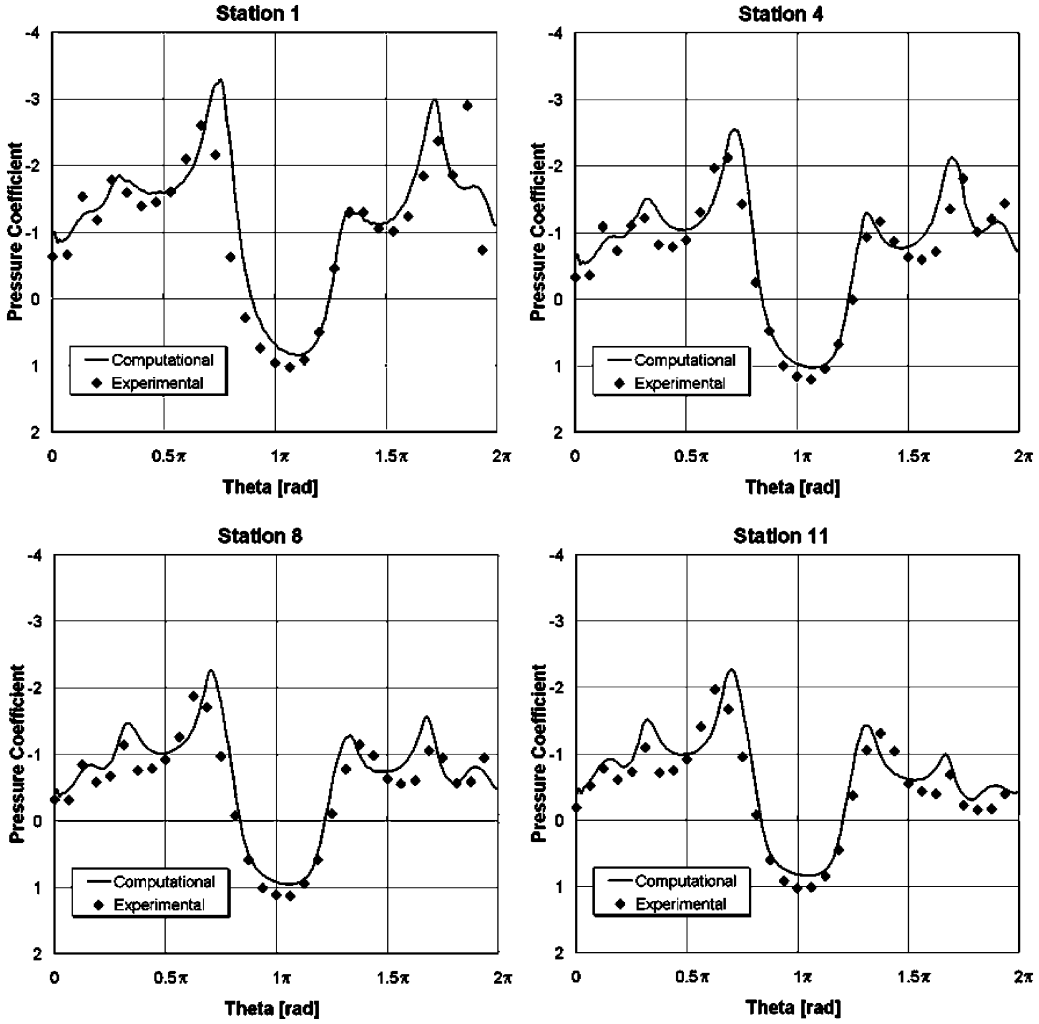

Fig. 5 Line plots of forebody pressure distribution for the square ogive at $\alpha = 60$ deg, $Re_D = 2.09 \times 10^6$, $M_\infty = 0.21$, and $\Omega b/(2V_\infty) = -0.20$. $\theta = 0$ deg is the top or leeside of the model. (See Fig. 2 for station locations and theta orientation.)

the grid-refinement study in an unsteady mode with a dynamically rotating grid.

The two grid-refinement cases have nominally two and four million points, corresponding to double and quadruple the number of points of the original grid. The original grid has an initial normal cell spacing corresponding to $y^+ \approx 40$. Although it is recommended that the initial normal cell spacing should correspond to $y^+ \approx 1$, such small spacing is not necessary when using an algebraic turbulence model like Baldwin–Lomax.[30] The grid with two million points has the same surface definition with more points in the normal direction corresponding to $y^+ \approx 1$. The grid with four million points has a more refined surface definition and maintains the refined normal spacing corresponding to $y^+ \approx 1$.

The original and two refined grids for the circular ogive geometry were simulated with OVERFLOW-D in a time-accurate mode with no rotational source term. In this mode the grid is no longer static, but rotates with an angular velocity corresponding to $\Omega b/(2V_\infty) = -0.1$. A nondimensional time step corresponding to a grid rotation of 0.01 deg is used for the time-accurate simulations. The forces and moments for the forebody region for the different grid sizes are compared in Table 3. The normal-force, axial-force, rolling-moment, and pitching-moment coefficients changed by less than 10% when using the refined grids. The side-force and yawing-moment coefficients both increased by roughly 30–40% relative to the values of the original grid, but changed by less than 10% between the two refined grid cases. Given the changes in the side-force and yawing-moment coefficients, the original grid might be slightly too coarse, but nonetheless, given the still relatively good agreement with experiments and limited computational resources, it is sufficient to demonstrate the capabilities of the flow solver. In many instances, the coarser baseline grid unexpectedly produced better results in terms of forces and moments. Some of the differences might be caused by the fact that the baseline simulations were computed in a static mode with source terms and the refined grid cases were computed in a dynamic mode without source terms. In theory, the two approaches should produce the same results; however, Potsdam and Strawn[31] have also noticed small differences in their CFD results between the two approaches.

OVERFLOW has several options for turbulence model. Among them are the Baldwin–Lomax algebraic model, Baldwin–Barth or Spalart–Allmaras one-equation model, and k-ω two-equation model.[32] Each model has its own advantages and disadvantages. For this study, the algebraic Baldwin–Lomax turbulence model with Degani–Schiff cutoff[33] is selected because its simplicity translates into significantly less computing time and resources. Two case studies were conducted to examine the effect of turbulence model on the forebody forces and moments. The circular ogive at $\Omega b/(2V_\infty) = -0.1$ and square ogive at $\Omega b/(2V_\infty) = -0.2$ cases are simulated using both the Baldwin–Lomax[18] and Spalart–Allmaras[19] turbulence models. The results are compared in Table 4. For the circular ogive case, the forebody side force and yawing-moment computed with Spalart–Allmaras are twice the magnitude of the Baldwin–Lomax results. For both cases, the Baldwin–Lomax turbulence model predicted forces and moments that more accurately matched experimental results. For these vortex-dominated flow conditions, the Baldwin–Lomax turbulence model with Degani–Schiff

Table 3 Comparison of forebody (see Fig. 2 for forebody definition) force and moment coefficients for the circular ogive at $\alpha = 60$ deg, $M_\infty = 0.21$, $Re_D = 2.08 \times 10^6$, and $\Omega b/(2V_\infty) = -0.10$ with different grid sizes

Force/moment coefficients	Original grid 1,270,000 points	Refined grid 2,450,000 points	Refined grid 4,310,000 points	Experiment
C_N	−0.1333	−0.1216	−0.1222	−0.1411
C_A	−4.0528	−4.0534	−4.0532	−4.0717
C_Y	0.0166	0.0221	0.0209	0.0193
C_l	0.0002	0.0002	0.0002	0.0002
C_m	0.2524	0.2328	0.2337	0.2624
C_n	0.0035	0.0050	0.0046	0.0037

Table 4 Comparison of forebody (see Fig. 2 for forebody definition) force and moment coefficients for simulations with either the Baldwin–Lomax or Spalart–Allmaras turbulence model

Force/moment coefficients	Circular ogive, $\Omega b/2V_\infty = -0.1$			Square ogive, $\Omega b/2V_\infty = -0.2$		
	Spalart–Allmaras	Baldwin–Lomax	Experiment	Spalart–Allmaras	Baldwin–Lomax	Experiment
C_N	−0.1980	−0.1400	−0.1411	−0.2177	−0.1904	−0.2166
C_A	−3.9391	−3.9478	−4.0717	−4.7419	−4.7448	−4.7797
C_Y	0.0309	0.0166	0.0193	0.0999	0.0786	0.0564
C_l	0.0002	0.0002	0.0002	−0.0002	−0.0002	−0.0001
C_m	0.3597	0.2612	0.2624	0.4069	0.3568	0.4078
C_n	0.0073	0.0035	0.0037	0.0277	0.0219	0.0156

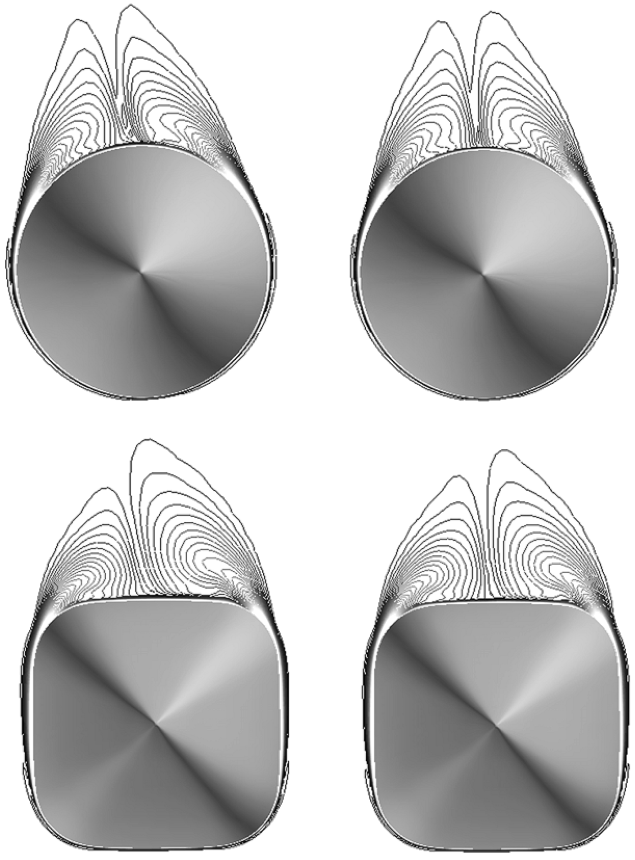

Fig. 6 Vorticity magnitudes at station 8 on the forebody (see Fig. 2 for station 8 location): left, $\Omega b/(2V_\infty) = -0.20$; right, $\Omega b/(2V_\infty) = -0.10$.

cutoff performs just as well if not better than the Spalart–Allmaras one-equation model.

In addition to choosing an appropriate turbulence model, the choice of numerical scheme can affect the CFD solution as well. The LU-SGS[16] and ARC3D[17] schemes were compared in this study. Table 5 indicates that the forces and moments are generally insensitive between these two numerical schemes. The largest difference between the two sets of results is that the side-force coefficient computed with the ARC3D scheme is 5% smaller.

Table 5 Comparison of forebody (see Fig. 2 for forebody definition) force and moment coefficients for the circular ogive at $\alpha = 60$ deg, $M_\infty = 0.21$, and $Re_D = 2.08 \times 10^6$, and $\Omega b/(2V_\infty) = -0.20$ simulated with either the LU-SGS or ARC3D numerical scheme

Force/moment coefficients	LU-SGS	ARC3D	Experiment
C_N	−0.1404	−0.1376	−0.1419
C_A	−3.9468	−3.9478	−4.0730
C_Y	0.0269	0.0257	0.0248
C_l	0.0002	0.0002	0.0002
C_m	0.2619	0.2578	0.2636
C_n	0.0065	0.0063	0.0054

All cases simulated are at Reynolds number above two million based on the diameter and freestream conditions. At that Reynolds number the flow is mostly turbulent, but small regions of laminar flow tend to remain, particularly near the nose tip, and might influence the global flow development. The prediction of transition in conjunction with a three-dimensional Reynolds-averaged Navier–Stokes flow solver remains difficult at this time. Without a transition model available, all cases are assumed to be fully turbulent at the 2×10^6 Reynolds-number flow condition.

Reasonable comparisons of computational results to experimental data suggest that the fully turbulent assumption is acceptable for the geometries and flow conditions studied here.

Conclusions

This study was motivated by the need of industry to quickly and inexpensively determine stability and control characteristics of new aircraft without solely having to resort to wind-tunnel experiments, which are difficult and expensive to conduct, especially if the tests are dynamic in nature. The potentially cheaper and faster aspects of computational fluid dynamics make it a helpful addition to experiments, if it can be proven to be reliable under dynamic conditions. To that end, a Reynolds-averaged Navier–Stokes flow solver, OVERFLOW, is applied to predict the flow characteristics about circular and square forebody models under rotary conditions.

Several cases are simulated at Reynolds numbers of approximately 2×10^6 and different rotation rates for two model geometries. The forebody results compared reasonably to the experimental pressure data in most cases. Additional study is needed to more accurately compute the flow in the mid and aft regions of the ogive.

Acknowledgments

The efforts of the first, second, and fourth author were supported by the NASA Langley Research Center under Grant No. NAG-1-2006 and Consortium Agreement NCC1-01-007. We would like to thank Roger Strawn, Mark Potsdam, Tor Nygaard, and William Chan of NASA Ames Research Center, Pieter Buning of NASA Langley Research Center, and Earl Duque of Northern Arizona University for their help and suggestions during the various stages of this project.

References

[1]Haines, A. B., "Scale Effects on Aircraft and Weapon Aerodynamics," AGARD-AG-323, July 1994.

[2]Polhamus, E. C., "A Review of Some Reynolds Number Effects Related to Bodies at High Angles of Attack," NASA CR 3809, Aug. 1984.

[3]Fluid Dynamics Panel Working Group 11, "Rotary-Balance Testing for Aircraft Dynamics," AGARD AR-265, Dec. 1990.

[4]Dunham, D. M., "Rotary Results on Forebody Models," Cooperative Programme on Dynamic Wind Tunnel Experiments for Maneuvering Aircraft, AGARD AR-305, Oct. 1996, pp. 7-1–7-14.

[5]Pauley, H., Ralston, J., and Dickes, E., "Experimental Study of the Effects of Reynolds Number on High Angle of Attack Aerodynamic Characteristics of Forebodies During Rotary Motion," NASA CR 195033, Jan. 1995.

[6]Spalart, P. R., "Strategies For Turbulence Modeling and Simulations," *International Journal of Heat and Fluid Flow*, Vol. 21, No. 3, 2000, pp. 252–263.

[7]Chaderjian, N. M., and Schiff, L. B., "Numerical Simulation of Forced and Free-to-Roll Delta Wing Motions," *Journal of Aircraft*, Vol. 33, No. 1, 1996, pp. 93–99.

[8]Sturek, W. B., Nietubicz, C. J., Sahu, J., and Weinacht, P., "Applications of Computational Fluid Dynamics to Aerodynamics of Army Projectiles," *Journal of Spacecraft and Rockets*, Vol. 31, No. 2, 1994, pp. 186–189.

[9]Weinacht, P., and Sturek, W. B., "Computation of Roll Characteristics of Finned Projectile," *Journal of Spacecraft and Rockets*, Vol. 33, No. 6, 1996, pp. 769–775.

[10]Weinacht, P., Sturek, W. B., and Schiff, L. B., "Navier–Stokes Predictions of Pitch Damping for Axisymmetric Projectiles," *Journal of Spacecraft and Rockets*, Vol. 34, No. 6, 1997, pp. 753–761.

[11]Weinacht, P., "Navier–Stokes Predictions of Individual Components of the Pitch-Damping Sum," *Journal of Spacecraft and Rockets*, Vol. 35, No. 5, 1998, pp. 598–605.

[12]Ludlow, D. K., and Qin, N., "Computational Prediction of Pitch Damping for Supersonic Blunt Cones," *Journal of Spacecraft and Rockets*, Vol. 35, No. 6, 1998, pp. 849–851.

[13]Ahmad, J., and Duque, E. P. N., "Helicopter Rotor Blade Computation in Unsteady Flows Using Moving Overset Grids," *Journal of Aircraft*, Vol. 33, No. 1, 1996, pp. 54–60.

[14]Nygaard, T. A., and Meakin, R. L., "An Aerodynamic Analysis of a Spinning Missile with Dithering Canards," AIAA Paper 2002-2799, June 2002.

[15]Buning, P. G., Jespersen, D. C., Pulliam, T. H., Chan, W. M., Slotnick, J. P., Krist, S. E., and Renze, K. J., "OVERFLOW User's Manual, Version 1.8," NASA Langley Research Center, Feb. 1998.

[16]Yoon, S., and Jameson, A., "Lower-Upper Symmetric Gauss-Seidel Method for the Euler and Navier–Stokes Equations," *AIAA Journal*, Vol. 26, No. 9, 1988, pp. 1025, 1026.

[17]Beam, R., and Warming, R., "An Implicit Factored Scheme for the Compressible Navier–Stokes Equations," *AIAA Journal*, Vol. 16, No. 4, 1978, pp. 393–402.

[18]Baldwin, B. S., and Lomax, H., "Thin Layer Approximation and Algebraic Model for Separated Turbulent Flows," AIAA Paper 78-257, Jan. 1978.

[19]Spalart, P. R., and Allmaras, S. R., "A One-Equation Turbulence Model for Aerodynamic Flows," AIAA Paper 92-0439, Jan. 1992.

[20]Ahmad, J. U., "Extension of OVERFLOW User's Manual to Rotorcraft Multidisciplinary Applications," NASA Ames Research Center, Aug. 1995.

[21]Srinivasan, G. R., Baeder, J. D., Obayashi, S., and McCroskey, W. J., "Flowfield of a Lifting Rotor in Hover: A Navier–Stokes Simulation," *AIAA Journal*, Vol. 30, No. 10, 1992, pp. 2371–2378.

[22]Park, M. A., and Green, L. L., "Steady-State Computation of Constant Rotational Rate Dynamic Stability Derivatives," AIAA Paper 2000-4321, Jan. 2000.

[23]Zhong, B., and Qin, N., "Non-Inertial Multiblock Navier–Stokes Calculation for Hovering Rotor Flowfields Using Relative Velocity Approach," *The Aeronautical Journal*, Vol. 105, No. 1049, July 2001, pp. 379–389.

[24]Chan, W. M., Rogers, S. E., Nash, S. M., Buning, P. G., and Meakin, R. L., "User's Manual for Chimera Grid Tools, Version 1.6," NASA Ames Research Center, Sept. 2001.

[25]Chan, W. M., "OVERGRID," *Handbook of Grid Generation*, edited by J. F. Thompson, B. K. Soni and N. P. Weatherill, CRC Press, Boca Raton, FL, 1999, Appendix A.

[26]Chan, W. M., Chiu, I., and Buning, P., "User's Manual for the HYPGEN Hyperbolic Grid Generator and the HGUI Graphical User Interface," NASA TM 108791, Oct. 1993.

[27]Dickes, E. G., Hultberg, R. S., and Ralston, J. N., "Report of Rotary Balance Wind Tunnel Testing on Generic Forebody Configurations Consisting of Pressure Measurements and Force and Moment Data Conducted at the Defense Research Agency Bedford/Farnborough Facilities," Bihrle Applied Research Rept. 92-5, Sept. 1992.

[28]Saephan, S., "Simulation of Forebody Flows at High Angle of Attack Rotary Conditions," M.S. Thesis, Dept. of Mechanical and Aeronautical Engineering, Univ. of California at Davis, June 2002.

[29]Ericsson, L. E., "Challenges in High Alpha Vehicle Dynamics," *Progress in Aerospace Sciences*, Vol. 31, No. 4, 1995, pp. 291–334.

[30]Chan, W. M., Reynaldo, G. J., Rogers, S. E., and Buning, P. G., "Best Practices in Overset Grid Generation," AIAA Paper 2002-3191, June 2002.

[31]Potsdam, M. A., and Strawn, R. C., "CFD Simulations of Tiltrotor Configurations in Hover," American Helicopter Society, June 2002.

[32]Kral, L. D., "Recent Experience with Different Turbulence Models Applied to the Calculation of Flow Over Aircraft Components," *Progress in Aerospace Sciences*, Vol. 34, No. 7–8, Nov.–Dec. 1998, pp. 481–541.

[33]Gee, K., Cummings, R. M., and Schiff, L. B., "Turbulence Model Effects on Separated Flow About A Prolate Spheroid," *AIAA Journal*, Vol. 30, No. 3, 1992, pp. 655–664.